Journal of Solid State Chemistry 181 (2008) 2501–2506

Contents lists available at ScienceDirect

Journal of Solid State Chemistry

journal homepage: www.elsevier.com/locate/jssc

Structure and oxide anion conductivity in $Ln_2(TO_4)O$ (Ln = La, Nd; T = Ge, Si)

Laura León-Reina [a], José M. Porras-Vázquez [b], Enrique R. Losilla [b], Laureano Moreno-Real [b], Miguel A.G. Aranda [b,*]

[a] Laboratorio de Difracción de Rayos-X, Servicios Centrales de Apoyo a la Investigación, Universidad de Málaga, 29071 Málaga, Spain
[b] Departamento de Química Inorgánica, Cristalografía y Mineralogía, Universidad de Málaga, 29071 Málaga, Spain

ARTICLE INFO

Article history:
Received 5 May 2008
Received in revised form
10 June 2008
Accepted 14 June 2008
Available online 18 June 2008

Keywords:
Oxide anion conductivity
p-type electronic conductivity
Neutron diffraction
Oxy-apatite

ABSTRACT

Oxy-silicate and oxy-germanate, $Ln_2(TO_4)O$ (Ln = La and Nd, T = Ge and Si) compounds have been prepared. Oxy-germanates can be readily obtained as highly crystalline single phases, while, the oxy-silicates are difficult to prepare as pure phases. The crystal structure of $Nd_2(SiO_4)O$ has been studied from a joint Rietveld refinement of neutron and laboratory X-ray powder diffraction data. The electrochemical characterisation indicates that these compounds display oxide anion conductivity with p-type electronic contribution under oxidising conditions. The apparent activation energies under dry flowing nitrogen, where p-type contribution is minimised, are 0.97(1), 1.05(3) and 1.17(4) eV, for $Nd_2(SiO_4)O$, $La_2(GeO_4)O$ and $Nd_2(GeO_4)O$, respectively. The overall conductivities at 1173 K range from 1.2×10^{-4} S cm^{-1} for $Nd_2(SiO_4)O$ to 1.3×10^{-6} S cm^{-1} for $La_2(GeO_4)O$. Finally, the stability of these compounds under very reducing conditions has been studied and partial degradation is reported.

1. Introduction

Over the last three decades, solid oxide fuel cells (SOFCs) have been attracting considerable interest because of their potential application as alternative electrical power generation systems with low emission of pollutants and high-energy conversion efficiency [1,2]. Yttria stabilised zirconia (YSZ), is the electrolyte used in the commercial systems due to its high oxide ion conductivity at elevated temperatures (1173–1273 K). However, there is a great interest in the development of devices with lower operational temperatures (873–1073 K) to overcome side problems including difficulties in cell sealing or low lifetime of the components caused by the high operation temperature [3]. For this purpose, ionic conductors with high conductivities at lower temperatures are strongly desired. Therefore, other electrolytes are being intensively studied: $Ce_{0.8}Gd_{0.2}O_{1.9}$ (GDC) [4]; $(Bi_2O_3)_{0.75}$–$(RE_2O_3)_{0.25}$ [5]; perovskite-type oxides like $La_{0.9}Sr_{0.1}Ga_{0.8}Mg_{0.2}O_3$ [6]; BIMEVOX $Bi_2V_{0.86}Ni_{0.14}O_{5.29}$ [7], and rare-earth oxy-apatites such as $La_{9.33}(SiO_4)_6O_2$ [8,9].

As part of the investigation of alternative structures, a new family of oxide ion conductors derived from La_2GeO_5 has been recently reported [10–12]. Neutron powder diffraction (NPD) data [12] showed that La_2GeO_5 is monoclinic (space group $P2_1/c$, $a = 9.604$ Å, $b = 7.469$ Å, $c = 7.112$ Å, $\beta = 107.55^\circ$ and $V = 486.4$ Å^3) and consists of isolated GeO_4 tetrahedra arranged in layers perpendicular to the a-axis. Lanthanum cations are located in two sites, one nine-coordinated, La(1) and another seven-coordinated, La(2). The La(2) position is located within the layers of GeO_4 tetrahedra while the La(1) ions are above and below the layers with the O(5) ion bridging the two La ions. Therefore, the structural formula of this compound can be formulated as $La_2(GeO_4)O$ to emphasise its oxy-germanate nature and weakly bonded oxide anions which display oxide conductivity properties. The reported ion conductivity for stoichiometric $La_2(GeO_4)O$ at 1173 K ranges between $\sim2\times10^{-4}$ [10] and $\sim5\times10^{-5}$ S cm^{-1} [12].

In order to increase oxide ion conductivity, Ishihara et al. [10] investigated $La_{2-x}GeO_{5-1.5x}$, $0.0\leqslant x\leqslant0.50$ series. The crystal structure was described as monoclinic $P2_1/c$ and the conductivity increased with the concentration of La vacancies, reaching a maximum at $x = 0.39$ in $La_{2-x}GeO_{5-1.5x}$. However, it is now understood that $La_{2-x}GeO_{5-1.5x}$ ($x = 0.44$) is equivalent to $La_{9.33}\square_{0.67}(GeO_4)_6O_2$ [12]. Therefore, introducing lanthanum vacancies in monoclinic $La_2(GeO_4)O$ leads to a structural change to produce materials with an oxy-apatite-type framework that is hexagonal for $x = 0.44$. For intermediate La/Ge ratios ($x = 0.33$–0.39), triclinic oxy-apatite is formed [13,14] which contains GeO_5 trigonal bipyramids [15,16], with the $x = 0.33$ member being $La_{10}[(GeO_4)_5(GeO_5)]O_2$.

On the other hand, lanthanum oxy-orthosilicate was first prepared by Toropov and Chih-ch'ung [17] who reported its X-ray powder data. The crystal structure of $La_2(SiO_4)O$ has been very recently refined from laboratory X-ray powder diffraction (LXRPD) [18] showing that $La_2(SiO_4)O$ is also monoclinic ($P2_1/c$, $a = 9.604$ Å, $b = 7.469$ Å, $c = 7.112$ Å, $\beta = 107.55^\circ$ and $V = 486.4$ Å^3).

* Corresponding author. Fax: +34 952132000.
E-mail address: g_aranda@uma.es (M.A.G. Aranda).

0022-4596/$ - see front matter © 2008 Elsevier Inc. All rights reserved.
doi:10.1016/j.jssc.2008.06.029

This material has received attention because of its application as a component of high-temperature resistant composites, dielectric materials, abrasives and as a part of a diode-pumped efficient laser [19]. To the best of our knowledge, there have been few investigations related to their solid-state synthesis and phase diagrams [20].

It has been reported [18] that $La_2(SiO_4)O$ can be prepared by solid-state reaction between La_2O_3 and SiO_2 at 1773 K for 1 day. An alternative mechanochemical synthetic method was also been published [21] allowing the formation of $La_2(SiO_4)O$ without any detectable traces of $La_{9.33}\square_{0.67}(SiO_4)_6O_2$ after heating at 1373 K for 2 h. However, no impedance studies of this set of compounds have been undertaken.

As part of our research project of oxy-silicates [22–24], oxy-germanates [25,26], and oxy-aluminates [27], we report here results for $Ln_2(TO_4)O$ (Ln = La, Nd; and T = Ge, Si) compounds. The crystal structure of $Nd_2(SiO_4)O$ has been analysed by NPD and electrochemical characterisation indicates a mixed oxide with p-type electronic conductivity.

2. Experimental

2.1. Synthesis

The nominal stoichiometries $La_2(GeO_4)O$, $Nd_2(GeO_4)O$, $La_2(SiO_4)O$ and $Nd_2(SiO_4)O$ were prepared by the ceramic method using high purity oxides: La_2O_3 and Nd_2O_3 (Alfa, 99.999%), GeO_2 (Aldrich, 99.998%) and SiO_2 (ABCR, quartz powder 99.31%). Lanthanum and neodymium oxides were pre-calcined at 1273 K for 2 h in order to achieve decarbonation. The precursors were mixed to prepare ~3 g batches by the following overall reaction:

$$Ln_2O_3 + TO_2 \xrightarrow{\Delta} Ln_2TO_5 \ (Ln = \text{La and Nd},\ T = \text{Ge and Si})$$

The starting mixtures were ground in an agate mortar for 15 min, pelletised and heated for 72 h in Pt crucibles at 1573 K for oxy-germanates and 1773 K for oxy-silicates. Weight losses, linked to Ge volatilisation, at these temperatures and times were found to be negligible.

2.2. Powder diffraction

All compounds were characterised by LXRPD at room temperature. The powder patterns were collected on a X'Pert Pro MPD automated diffractometer equipped with a Ge(111) primary monochromator (strictly monochromatic Cu$K\alpha_1$ radiation) and an X'Celerator detector. The measurement time was ~4 h per pattern to obtain very good statistics over the 2θ range 5–145° with a 0.017° step size. All Rietveld [28] analyses were carried out by using the GSAS suite of programs [29].

Room temperature NPD patterns were collected on HRPT diffractometer [30] [SINQ neutron source at Paul Scherrer Institut, Villigen, Switzerland] for $Nd_2(SiO_4)O$ loaded in a vanadium can. The neutron wavelength (~1.886 Å) was selected by the (511) reflection of the vertically focusing Ge monochromator. Data collection required ~6 h per pattern to have good statistics over the 2θ range 10–160° [10.82–0.9 Å] with a 0.05° step size. The structure parameters for $Nd_2(SiO_4)O$ were obtained from the joint Rietveld refinement of LXRPD and NPD using the GSAS [29].

2.3. Electrical measurements

Impedance data were collected on cylindrical pellets (~10 mm diameter and ~1 mm thickness) obtained by pressing the fine powder at 400 MPa, for 1 min. The pellets were sintered to allow densification and to increase the mechanical strength, at 1923 K for 6 h for oxy-silicates and 1623 K for 96 h for oxy-germanates. The pellets were not fully dense and the compactions were ~95% for $Ln_2(SiO_4)O$ and ~80% for $Ln_2(GeO_4)O$. These values were calculated taking into account the pellet mass and volume, and the crystallographic density for each compound. No weight losses were detected in this sintering step, which was monitored by weighting the pellets before and after the thermal treatment. Electrodes were made by coating opposite pellet faces with METALOR® 6082 platinum paste and heating to 1223 K at a rate of 10 K min^{-1} in air to decompose the paste and harden the Pt residue. Successive treatments were made to achieve an electrical resistance of both pellets faces lower than 1 Ω.

Impedance spectroscopy data were collected in three different flowing atmospheres (dry nitrogen, dry synthetic air and dry oxygen) using a Hewlett-Packard 4284A impedance analyser over the frequency range 20 Hz–1 MHz with an applied voltage of 1 V from 573 to 1273 K for all the samples. Measurement processes were electronically controlled by the winDETA programme package [31]. The pellets were mounted in a homemade alumina conductivity jig, with four Pt wires shielded in two alumina tubes, which were placed in a tube furnace. Electrical data were taken every 50 K. A delay time of 60 min at each temperature was selected to ensure thermal equilibrium. Temperatures were reproducible to ±1 K.

3. Results and discussion

3.1. Synthesis and phase assemblage

$Ln_2(TO_4)O$ (Ln = La and Nd, T = Ge and Si) compounds, have been obtained as crystalline compounds by solid-state reaction. The dominant phase in our synthetic conditions is the monoclinic $La_2(GeO_4)O$-type structure. LXRPD patterns for $Ln_2(GeO_4)O$ (Ln = La and Nd) showed that these materials were single phase. LXRPD patterns for $Ln_2(SiO_4)O$ (Ln = La and Nd) compounds indicated the presence of hexagonal oxy-apatite $Ln_{9.33}(SiO_4)_6O_2$ as an impurity phase. The analysis of the LXRPD data by the Rietveld method showed that $La_2(SiO_4)O$ and $Nd_2(SiO_4)O$ samples contained 16.6(2) and 3.6(1) wt% of oxy-apatite, respectively (see Table 1). The room temperature unit cell data are also given in Table 1. As expected, the oxy-germanates have larger volumes

Table 1
Secondary phase yield, Rietveld factor (R_{wp}) and refined unit cell parameters for $Ln_2(TO_4)O$ (Ln = La, Nd; T = Ge, Si) at room-temperature in $P2_1/c$ symmetry

Sample	Impurity (wt%)[a]	R_{wp} (%)	a (Å)	b (Å)	c (Å)	β (deg)	V (Å^3)
$La_2(GeO_4)O$	–	5.60	9.6072(1)	7.4687(1)	7.1137(1)	107.542(1)	486.70(1)
$Nd_2(GeO_4)O$	–	3.25	9.4507(1)	6.9824(1)	7.2633(1)	106.447(1)	459.67(1)
$La_2(SiO_4)O$	16.6(2)	7.30	9.3232(1)	7.5043(1)	7.0291(1)	108.668(1)	465.91(1)
$Nd_2(SiO_4)O$	3.6(1)	3.58	9.2300(1)	7.2831(1)	6.8749(1)	108.191(1)	439.06(1)

[a] The impurities are lanthanide oxy-apatites.

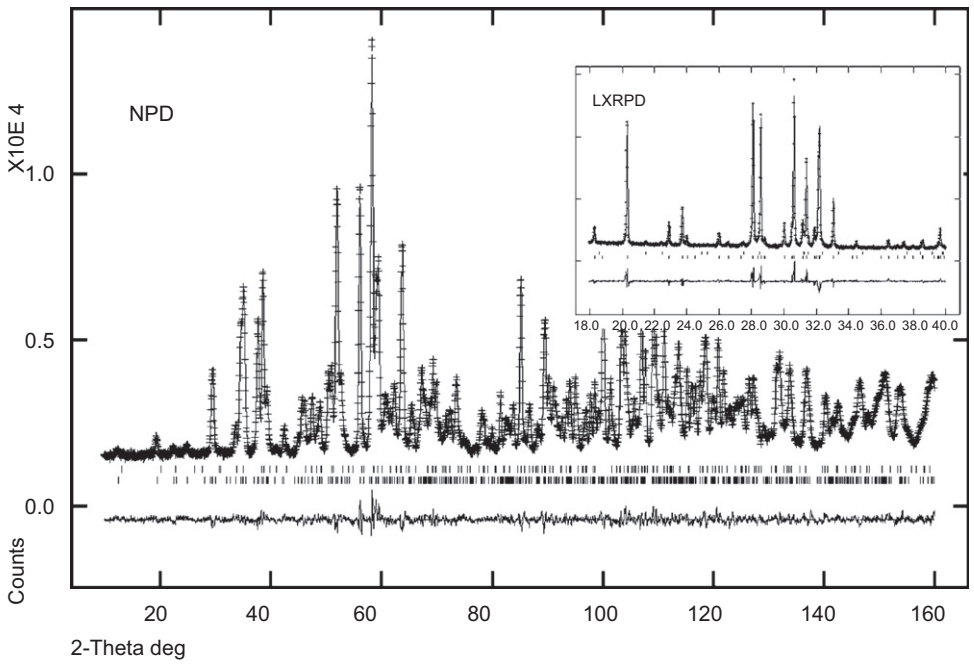

Fig. 1. Observed (crosses), calculated (full line) and difference (bottom) NPD patterns ($\lambda = 1.89$ Å) for $Nd_2(SiO_4)O$ at room-temperature. The inset shows a selected region of the LXRPD ($\lambda = 1.54$ Å) Rietveld plot for the same sample at the same temperature.

than the corresponding oxy-silicates, and the unit cell volumes for La^{3+} oxy-salts are dilated compared to the Nd^{3+} analogues due to the differences in ionic radii [32].

3.2. Crystal structures

The crystal structure of $Nd_2(SiO_4)O$ was studied in detail by the combination of LXRPD and NPD. Powder diffraction patterns were analysed by using a *pseudo*-Voigt peak shape function with the asymmetry correction included. The refined overall parameters were: background coefficients, cell parameters, zero-shift error and peak shape parameters, and included minor neodymium oxy-apatite, $Nd_{9.33}(SiO_4)_6O_2$ (ICSD no. 55100). The fit was very good and the Rietveld plots are shown in Fig. 1. The final unit cell parameters, *R*-values and refined atomic parameters are given in Table 2. Selected interatomic bond distances and angles are listed in Table 3.

The crystal structure of $Nd_2(SiO_4)O$ consists, as previously reported [18] for $La_2(SiO_4)O$, of three types of polyhedra: $Nd(1)O_9$, $Nd(2)O_7$ and SiO_4 (Fig. 2). The ionic radius of Nd^{3+} in nine-fold coordination (1.163 Å) and that of Nd^{3+} in seven-fold coordination (1.046 Å) [32] would yield average interatomic distances of 2.583 and 2.466 Å for Nd(1)–O and Nd(2)–O, respectively. These predicted values are in very good agreement with the corresponding mean interatomic distances (Table 3). On the other hand, the SiO_4 tetrahedron is quite regular with the expected bond distances (see Table 3). The bond valence sum [33] for all atoms are also given in Table 3. It must be noted that O(3) is surrounded by three neodymium atoms at long distances and one silicon atom. Due to the long Nd–O(3) distances, the resulting bond valence sum for this atom is rather small, 1.76. This under-valence justifies the short Si–O(3) bond (Table 3). In order to investigate the (possible) presence of oxide vacancies, the occupation factors of all oxide anions were allowed to vary. The five occupation factors converged within the 0.98(1)–1.01(1) range. Therefore, we can rule out the presence of oxide vacancies in $Nd_2(SiO_4)O$ within the accuracy of this study, 1–2%.

Table 2
Unit cell parameters, *R*-factors and atomic parameters at room-temperature for $Nd_2(SiO_4)O$ ($P2_1/c$), from joint neutron and X-ray powder diffraction Rietveld refinement

a (Å)	9.2295(1)		R^X_{wp}/R^N_{wp} (%)	4.00/3.73
b (Å)	7.2848(1)		R^X_p/R^N_p (%)	2.70/2.93
a (Å)	6.8744(1)		R^X_F/R^N_F (%)	4.03/1.76
β (deg)	108.199(1)			
V (Å^3)	439.08(1)			
Atom	x	y	z	$U_{iso} \times 100$ (Å^2)
Nd(1)	0.3884(1)	0.1502(2)	0.5922(2)	0.75
Nd(2)	0.0172(1)	0.1236(1)	0.7340(2)	0.34
Si	0.2938(3)	0.5836(3)	0.5428(4)	0.41
O(1)	0.2938(3)	0.0701(4)	0.8649(4)	0.74
O(2)	0.3648(3)	0.4633(4)	0.7518(4)	0.63
O(3)	0.4078(3)	0.7553(4)	0.5570(4)	0.79
O(4)	0.1183(3)	0.6342(4)	0.4969(4)	0.75
O(5)	0.1138(3)	0.1248(4)	0.4526(3)	0.70

Table 3
Selected interatomic bond distances (Å), angles (deg) and bond valence sum for $Nd_2(SiO_4)O$

Nd(1)–O(1)	2.374(3)	Nd(2)–O(1)	2.458(3)	Si–O(1)	1.650(3)
Nd(1)–O(1)	2.549(3)	Nd(2)–O(4)	2.537(3)	Si–O(2)	1.630(3)
Nd(1)–O(2)	2.569(3)	Nd(2)–O(4)	2.440(3)	Si–O(3)	1.593(4)
Nd(1)–O(2)	2.581(2)	Nd(2)–O(4)	2.571(3)	Si–O(4)	1.632(3)
Nd(1)–O(2)	2.427(3)	Nd(2)–O(5)	2.369(3)	O(1)–Si–O(2)	101.7(2)
Nd(1)–O(3)	2.897(3)	Nd(2)–O(5)	2.327(3)	O(1)–Si–O(3)	116.5(2)
Nd(1)–O(3)	2.665(3)	Nd(2)–O(5)	2.361(3)	O(1)–Si–O(4)	102.8(2)
Nd(1)–O(3)	2.503(3)	⟨Nd(2)–O⟩	2.44	O(2)–Si–O(3)	108.1(2)
Nd(1)–O(5)	2.420(2)			O(2)–Si–O(4)	111.9(2)
⟨Nd(1)–O⟩	2.55			O(3)–Si–O(4)	115.1(2)
Nd(1)	2.86	Nd(2)	2.92	Si	3.98
O(1)	2.10	O(2)	1.96	O(3)	1.76
O(4)	1.98	O(5)	1.97		

Fig. 2 shows two projections of the crystal structure of $Nd_2(SiO_4)O$. It is worth pointing out that the non-framework oxide anions, O(5), are stacked along the *a*-axis (Fig. 2a), and that

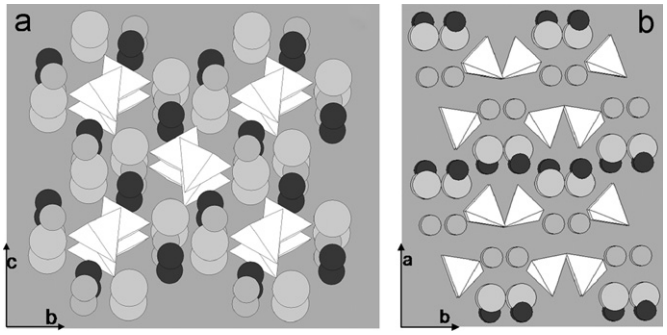

Fig. 2. Crystal structure of $Nd_2(SiO_4)O$ with the SiO_4 groups shown as tetrahedra, oxide anions as large spheres, and neodymium cations as small spheres: Nd(1) and Nd(2) are white and black, respectively: (a) projection viewed down *a*-axis and (b) projection viewed down *c*-axis.

the atomic displacement parameter for O(5) is comparable to those of the oxide anions belonging to the silicate tetrahedron (Table 2). This behaviour could suggest that the oxide conductivity (see below), may be due to a high-temperature cooperative bond breaking and re-forming between O(5) and the SiO_4 tetrahedra as reported for other families of oxy-salts with tetrahedral moieties, such as $La_{0.8}Ba_{1.2}GaO_{3.9}$ [34] and $Ca_{12}(Al_{14}O_{32})O$ [35]. However, structural studies at high temperature combined with modelling techniques are needed to establish the oxide conductivity mechanism for this family of oxy-silicates and oxy-germanates.

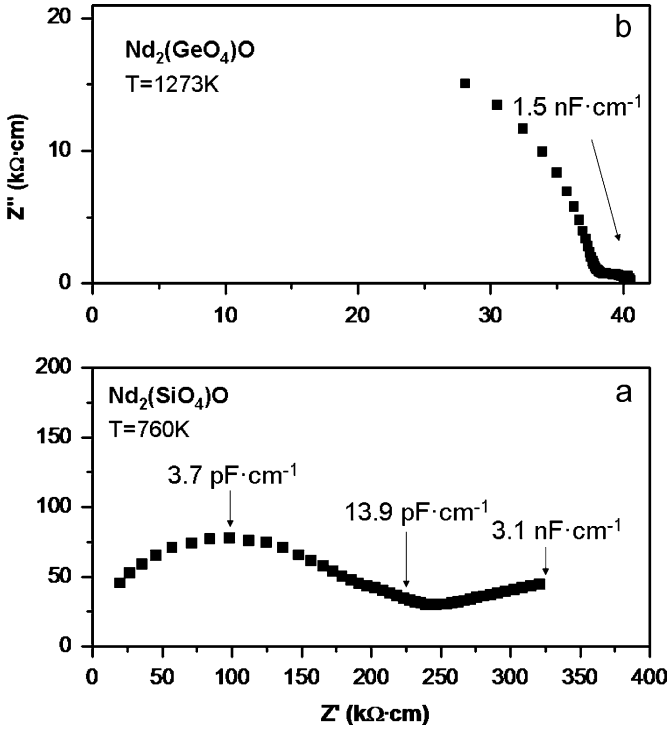

Fig. 3. Complex impedance plane plot data collected under flowing dry air, with selected associated capacitances highlighted, for (a) $Nd_2(SiO_4)O$ at 760 K, and (b) $Nd_2(GeO_4)O$ at 1273 K.

3.3. Electrical characterisation

Some results from the impedance study of $Ln_2(TO_4)O$ (Ln = La and Nd, T = Ge and Si) are shown in Figs. 3 and 4. Complex impedance plane plots for $Nd_2(SiO_4)O$ and $Nd_2(GeO_4)O$ are given in Fig. 3 as representatives of the family. The pattern for $Nd_2(SiO_4)O$ at 760 K shows at least two semicircles plus the electrode contribution (Fig. 3a), with likely contributions being a grain interior response (bulk) and internal interfaces (grain boundary and porosity). Lower frequency processes are observed in the form of a spike with associated capacitances close to 1 nF cm^{-1}, but collapse at high temperatures as shown for $Nd_2(GeO_4)O$ at 1273 K (Fig. 3b). From these data, it may be concluded that the samples show ionic conductivity as previously reported for La_2GeO_5 [10–12].

Overall pellet conductivities (σ_T) are obtained from the intercept of the spikes and/or the arcs (low-frequency ends) on the Z'-axis, and they are given in the traditional Arrhenius representation (Fig. 4). Conductivity data for $La_2(SiO_4)O$ are not reported as the pellets contain approximately 17 wt% of lanthanum oxy-apatite. The conductivity data for $Nd_2(SiO_4)O$ and $Ln_2(GeO_4)O$ (Ln = Nd, La) were recorded under three flowing dry atmospheres (Fig. 4), because in the experiment of σ_T vs. $p(O_2)$, very reducing conditions (see Experimental section) led to sample degradation as discussed below.

Fig. 4a shows σ_T values for $Nd_2(SiO_4)O$ under N_2, synthetic air and O_2 atmospheres, and fall on a set of straight lines with higher conductivity as the oxygen partial pressure increases. This behaviour is typical of ionic conductors with a p-type electronic contribution. In order to assess this hypothesis, overall conductivity values, at constant temperature, were re-plotted as function of the oxygen partial pressure (Fig. 4c). The three points are linear with a slope of 0.23(1), and is very close to the expected slope for a p-type electronic conductor (0.25). Therefore, it can be concluded that $Nd_2(SiO_4)O$ is an ionic conductor with a significant p-type electronic contribution. The apparent activation energies from reducing to oxidising conditions are 0.97(1), 0.94(1) and 0.85(1) eV decrease as the electronic contribution increases. The activation energy under nitrogen (0.97(1) eV), is typical for oxide conductors. Finally, the overall conductivity for $Nd_2(SiO_4)O$ under nitrogen at 1173 K was 1.2×10^{-4} S cm^{-1}.

Fig. 4b shows σ_T values for $Ln_2(GeO_4)O$ (Ln = Nd, Ge) also under N_2, synthetic air and O_2 atmospheres. Firstly, it must be noted that $Nd_2(GeO_4)O$ conductivity is larger than that of $La_2(GeO_4)O$ although the different compactions of the pellets, 85% vs. 70%, may play a role. Secondly, and as previously discussed for $Nd_2(SiO_4)O$, overall conductivities increase as the oxygen partial pressure increases. Therefore, p-type electronic conductivity seems to be a common feature of this family of compounds. Conductivity data at 1173 K has been re-plotted as function of the oxygen partial pressure in Fig. 4d, but the variation is non-linear because the conductivity under N_2 is nearly pure ionic. To test this hypothesis, we have determined the slope of the straight lines derived only from the first two points being 0.29 and 0.24 for $Nd_2(GeO_4)O$ and $La_2(GeO_4)O$, respectively. These values are quite close to 0.25, and therefore, the presence of p-type electronic contribution in these oxy-germanates is also established. The apparent activation energies from reducing to oxidising conditions are 1.17(4), 1.09(2) and 1.08(2) eV for $Nd_2(GeO_4)O$ and 1.05(3), 1.09(2) and 1.05(3) eV for $La_2(GeO_4)O$. Finally, the overall conductivities value for $Nd_2(GeO_4)O$ and $La_2(GeO_4)O$ under nitrogen at 1173 K were 3.7×10^{-6} and 1.3×10^{-6} S cm^{-1}, respectively.

The stability of $Ln_2(TO_4)O$ compounds were studied by treating the pelletised samples at 1173 K for 24 h under two atmospheres, pure dry N_2 and dry 5%H_2–Ar, after which the pellets were ground and LXRPD patterns collected. The samples were stable under a dry N_2 flux, but partially decomposed under dry 5%H_2–Ar. Fig. 5 shows the patterns before and after this last treatment for $Nd_2(SiO_4)O$ and $Nd_2(GeO_4)O$ as representatives of oxy-silicate and oxy-germanates, respectively; the former decomposed slightly to Nd_2O_3, while the degradation of $Nd_2(GeO_4)O$ to give

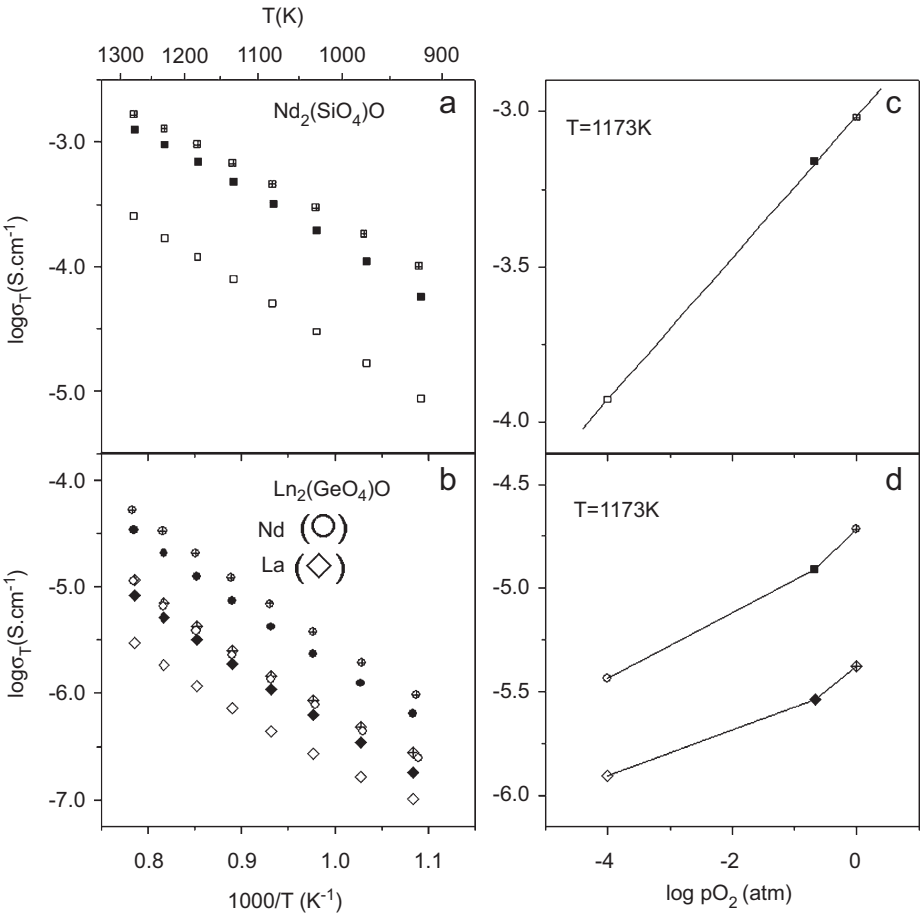

Fig. 4. (a) Arrhenius plots of $\log(\sigma_T)$ for $Nd_2(SiO_4)O$ (99% compaction). (b) Arrhenius plots of $\log(\sigma_T)$ for $Ln_2(GeO_4)O$ (Ln = Nd: 85% compaction, circles; Ln = La: 70% compaction, diamonds). Conductivity data are given for three types of flowing atmospheres: open symbols for dry nitrogen; full symbols for dry air; crossed symbols for dry oxygen. (c) $\log(\sigma_T)$ vs. $\log(pO_2)$ for $Nd_2(SiO_4)O$ at 1173 K. (d) $\log(\sigma_T)$ vs. $\log(pO_2)$ for $Ln_2(GeO_4)O$ (Ln = Nd [o], La [◇]) at 1173 K.

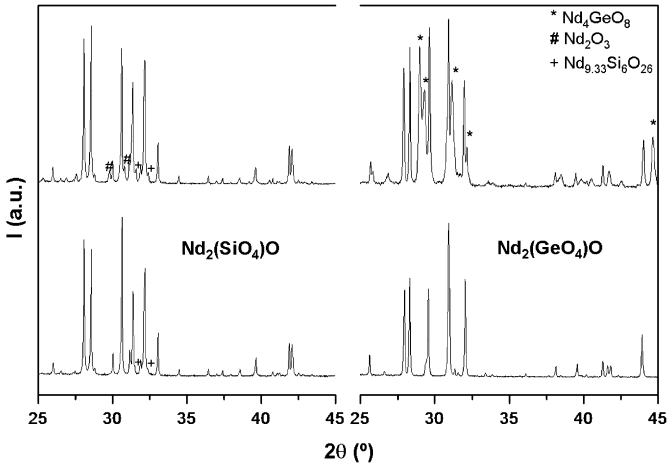

Fig. 5. X-ray powder diffraction patterns for $Nd_2(SiO_4)O$ (left) and $Nd_2(GeO_4)O$ (right). The bottom patterns correspond to as-synthesised samples, while the top patterns are obtained from partially decomposed pellets treated at 1173 K for 24 h under dry 5%H_2–Ar.

Nd_4GeO_8 was significant. This degradation, under reducing conditions, is likely due to Ge/Si volatilisation. Furthermore, this behaviour has been previously reported in germanium oxy-apatite systems.

A previous report [10] of conductivity versus pO_2 for $La_{2-x}GeO_{5-1.5x}$ ($0.17 \leqslant x \leqslant 0.39$) did not include data for La_2GeO_5. We now believe the authors did not report this curve because the sample decomposed under very reducing conditions, although, this was not explicitly stated. Furthermore, the flat curves reported for $La_{2-x}GeO_{5-1.5x}$ were very likely obtained for oxy-apatites and incorrectly assigned as arising from monoclinic La_2GeO_5-type compounds.

The ionic conductivity values for $Ln_2(TO_4)O$-type compounds are smaller than for YSZ and oxy-apatites. Attempts to introduce lanthanum vacancies to increase the conductivity led to the formation of oxy-apatite as an impurity phase. This behaviour has been already described [12], but disagrees with earlier reports [10,11] claiming that lanthanum vacancies were stable within the $Ln_2(TO_4)O$-type structure and enhance ionic conductivity. These improvements in the conductivity are now re-interpreted as arising from the presence of the oxy-apatite phase. Finally, the possibility of enhancing ion mobility by doping with small amounts of an alkali earth cation in order to introduce interstitial oxygens, $Ln_{2-x}M_x(TO_4)O_{1+x/2}$, remains to be investigated.

4. Conclusions

$Ln_2(TO_4)O$ (Ln = La and Nd, T = Ge and Si) compounds have been prepared and the crystal structure of $Nd_2(SiO_4)O$ derived from a joint Rietveld refinement of neutron and LXRPD. Electrochemical characterisation indicates that these compounds display both p-type electronic and oxide anion conductivities. We conclude that $Ln_2(TO_4)O$-type materials are not good candidates for electrolyte in SOFCs because they exhibit (i) low ionic conductivities (close or lower than 10^{-4} S cm^{-1} at 1173 K);

(ii) p-type electronic conductivity; and (iii) show degradation under a reducing atmosphere.

Supplementary material

Further details of the crystal structure investigation can be obtained from the Fachinformationszentrum Karlsruhe, 76344 Eggenstein-Leopoldshafen, Germany (fax: (49) 7247-808-666; e-mail: crysdata@fiz.karlsruhe.de) on quoting the depository number CSD-419456.

Acknowledgments

The work in Málaga has been supported by the MAT2006-11080-C02-01 research grant. JMPV thank MEC (Spain) for a studentship. This work was partially performed at the spallation neutron source SINQ, Paul Scherrer Institut, Villigen, Switzerland.

References

[1] B.C.H. Steele, A. Heinzel, Nature 414 (2001) 345–352.
[2] R.M. Ormerod, Chem. Soc. Rev. 32 (2003) 17–28.
[3] J.M. Ralph, A.C. Schoeler, M. Krumpelt, J. Mater. Sci. 36 (2001) 1161–1172.
[4] R.S. Torrens, N.M. Sammes, G.A. Tompsett, Solid State Ionics 111 (1998) 9–15.
[5] N.M. Sammes, G.A. Tompsett, H. Nafe, F. Aldinger, J. Eur. Ceram. Soc. 19 (1999) 1801–1826.
[6] T. Ishihara, H. Matsuda, Y. Takita, J. Am. Chem. Soc. 116 (1994) 3801–3803.
[7] F. Krok, I. Abrahams, D. Bangobango, W. Bogusz, J.A.G. Nelstrop, Solid State Ionics 111 (1998) 37–43.
[8] S. Nakayama, T. Kageyama, H. Aono, Y. Sadaoka, J. Mater. Chem. 5 (1995) 1801–1805.
[9] L. León-Reina, E.R. Losilla, M. Martínez-Lara, S. Bruque, A. Llobet, D.V. Sheptyakov, M.A.G. Aranda, J. Mater. Chem. 15 (2005) 2489–2498.
[10] T. Ishihara, H. Arikawa, T. Akbay, H. Nishiguchi, Y. Takita, J. Am. Chem. Soc. 123 (2001) 203–209.
[11] T. Ishihara, H. Arikawa, H. Nishiguchi, Y. Takita, Solid State Ionics 154–155 (2002) 455–460.
[12] P. Berastegui, S. Hull, F.J. García, J. Grins, J. Solid State Chem. 168 (2002) 294–305.
[13] L. León-Reina, M.C. Martín-Sedeño, E.R. Losilla, A. Cabeza, M. Martínez-Lara, S. Bruque, F.M.B. Marques, D.V. Sheptyakov, M.A.G. Aranda, Chem. Mater. 15 (2003) 2099–2108.
[14] L. León-Reina, J.M. Porras-Vazquez, E.R. Losilla, M.A.G. Aranda, J. Solid State Chem. 1180 (2007) 1250–1258.
[15] S.S. Pramana, W.T. Klooster, T.J. White, Acta Crystallogr. B 63 (2007) 597–602.
[16] S.S. Pramana, W.T. Klooster, T.J. White, J. Solid State Chem. (2008) on-line.
[17] N.A. Toropov, M. Chih-ch′ung, Bull. Acad. Sci. USSR Div. Chem. Sci. 12 (1963) 1918–1921.
[18] K. Fukuda, T. Iwata, Powder Diffraction 21 (2006) 300–303.
[19] J. Du, X. Liang, Y. Xu, R. Li, G. Zhao, C. Yan, L. Su, J. Xu, Z. Xu, Chinese Opt. Lett. 5 (2007) 172–174.
[20] Phase equilibria diagrams, The American Ceramic Society, NIST (ISBN: 0-944904-93-9).
[21] G. Tzvetkov, N. Minkova, J. Mater. Sci. 35 (2000) 2435–2441.
[22] L. León-Reina, E.R. Losilla, M. Martínez-Lara, S. Bruque, M.A.G. Aranda, J. Mater. Chem. 14 (2004) 1142–1149.
[23] J.M. Porras-Vázquez, A.G. De la Torre, E.R. Losilla, M.A.G. Aranda, Solid State Ionics 178 (2007) 1073–1080.
[24] J.M. Porras-Vázquez, E.R. Losilla, L. León-Reina, M. Martínez-Lara, M.A.G. Aranda, Chem. Mater. 20 (2008) 2026–2034.
[25] L. León-Reina, E.R. Losilla, M. Martínez-Lara, M.C. Martín-Sedeño, S. Bruque, P. Núñez, D.V. Sheptyakov, M.A.G. Aranda, Chem. Mater. 17 (2005) 596–600.
[26] L. León-Reina, J.M. Porras-Vázquez, E.R. Losilla, M.A.G. Aranda, Solid State Ionics 177 (2006) 1307–1315.
[27] L. Palacios, A. Cabeza, S. Bruque, S. Garcia-Granda, M.A.G. Aranda, Inorg. Chem. 47 (2008) 2661–2667.
[28] H.M. Rietveld, J. Appl. Crystallogr. 2 (1969) 65–71.
[29] A.C. Larson, R.B. von Dreele, GSAS program, Los Alamos National Laboratory, 1994 Rep. no. LA-UR-86748.
[30] P. Fischer, G. Frey, M. Koch, M. Konnecke, V. Pomjakushin, J. Schefer, R. Thut, N. Schlumpf, R. Burge, U. Greuter, S. Bondt, E. Berruyer, Physica B 276–278 (2000) 146–147.
[31] Novocontrol GmbH, WinDETA, Hundsangen, Germany, 1995.
[32] R.D. Shannon, Acta Crystallogr. A 32 (1976) 751–767.
[33] I.D. Brown, D. Altermat, Acta Crystallogr. B 41 (1985) 244–247.
[34] E. Kendrick, J. Kendrick, K.S. Knight, M.S. Islam, P.R. Slater, Nat. Mater. 6 (2007) 871.
[35] P.V. Sushko, A.L. Shluger, K. Hayashi, M. Hirano, H. Hosono, Phys. Rev. B 73 (2006) 014101.